Resonant Laser Manipulation of an Atomic Beam

T. C. Lilly[a], A. D. Ketsdever[a] and S. F. Gimelshein[b]

[a] *University of Colorado, 1420 Austin Bluffs Parkway UH 231, Colorado Springs, CO 80933*
[b] *ERC Inc., 10 E Saturn Blvd., Edwards AFB, CA 95324*

Abstract. Theories for laser-atom interactions have been under development since the advent of laser technology. The theories have yet to be adequately integrated into kinetic flow solvers. Realizing this integration would greatly enhance the scaling of laser-species interactions beyond the realm of ultra-cold atomic physics. A representative numerical investigation was conducted using a custom collisionless gas particle trajectory code, demonstrating this goal in the present study. The investigation covered neutral atomic beam steering and collimation using near-resonant laser fields. In addition to the numerical investigation, a validating experiment was conducted. The experimental results showed good agreement with the numerical simulations when experimental parameters, such as finite laser line width, were taken into account. These simulations showed trends and some limitations associated with the use of a continuous-wave Gaussian laser fields for the steering and collimation of a geometrically skimmed cesium atomic beam using the photon scattering force and the near-resonant induced dipole gradient force. These simulations indicate possible integration of the resonant laser-atom interaction with other rarefied and collisional solvers for similar species such as alkali metals.

Keywords: atomic beam, cesium, resonant laser, induced dipole, photon scattering
PACS: 37.10.Vz, 37.10.Mn, 37.10.De

INTRODUCTION

One application which benefits from the precision of laser-based atomic beam manipulation is micro-machining and micro-engineering. The key parameter in micro applications is the ability to affect a target flow over length scales which push the limits of physical manufacture. The ability to create masks, beam blocks, controlling electric fields, and other material-based flow interaction devices, is hindered on these scales; while, the ability to shape light at such scales is routine. Electromagnetic processes are currently used to ionize and direct an ionic flow for etching and deposition; these processes suffer from ionic particle-particle interactions and difficulty maintaining a neutral environment. With laser manipulation methods, the precision and characteristics of the flow control is limited only by one's ability to control the laser field without the necessity of ionizing the species. This study demonstrates an example of simulating the steering and collimation of a cesium atomic beam by resonant laser fields. The methodology demonstrated in this study can be adapted for designing full-scale systems for: micro-machining, micro-engineering, and lithography. The methodology can also be used for predicting the level of flow control capable by integrating laser control into existing systems.

Laser interactions with neutral atomic beams offer a strong, tunable method for the remote control of the beam's position and transverse temperature. So far the use of laser-atom manipulation has been primarily limited to low-temperature atomic physics, where resonant laser interactions offer the ability to cool [1], confine [2], and interrogate atoms with sub-micron precision [3]. The theory and techniques developed for these "cold" applications can be extended to include intense laser fields for steering and collimating flows with higher densities and energies than current common practice. One impediment to this extension is the development of a methodology for investigating the design space of potential laser modification scenarios beyond a single laser-atom interaction, i.e. integrating the interaction into a numeric kinetic flow solver. In this study, a methodology for such an investigation has been demonstrated by integrating resonant laser field interactions into a custom particle trajectory code.

THEORETICAL FRAMEWORK

Consistent with [4], the force on an atom in the laser propagation direction, due to the photon scattering force from a near resonant laser field, is given by

$$F_{\text{scat}} = \frac{\hbar k s_0 \Gamma}{2}\left[1 + s_0 + \left(2\delta/\Gamma\right)^2\right]^{-1} \tag{1}$$

where $\hbar$ is Plank's constant over 2 pi, k is the laser wavenumber, s_0 is the on-resonance saturation parameter, defined as laser intensity divided by the saturation intensity, δ is the laser detuning from the transition frequency, and Γ is the natural frequency width of the transition. Note, the inverse of the natural width, $1/\Gamma$, defines the excited state decay lifetime. This force is caused by the absorption and subsequent spontaneous emission of a photon. While absorption and stimulated emission exactly cancel the momentum exchange from the laser to the atom, the isotropic nature of spontaneous emission causes the atom to gain one photon momentum each absorption/emission cycle. Equation (1) addresses the asymptotic behavior of the force with increasing laser power ($s_0 \to \infty$). The asymptote is equal to one photon momentum ($\hbar k$) divided by twice the lifetime. This results from an average steady state excited population of ½ in a strong laser field, due to continual absorption and stimulated emission.

$$F_{\text{scat}}\big|_{\max} = \frac{\hbar k \Gamma}{2} \tag{2}$$

Also consistent with [4], the force on an atom in the radial laser direction, due to the induced dipole force associated with a near resonant laser field, is given by

$$F_{\text{dip}} \cong -\frac{\partial\ \Delta\varepsilon_g}{\partial r} = -\frac{\partial}{\partial r}\left(\frac{\hbar\Omega^2}{4\delta}\right) = -\frac{\hbar\Omega}{2\delta}\frac{\partial\Omega}{\partial r} = -\frac{1}{8}\frac{\hbar\Gamma^2}{\delta I_{\text{sat}}}\frac{\partial I(r)}{\partial r} \tag{3}$$

where $\Delta\varepsilon_g$ is the ground state Stark shift, Ω is the Rabi frequency (related to intensity), I_{sat} is the saturation intensity of the transition, and $I(r)$ is the radial intensity profile of the laser field. This force is derived from a gradient in potential energy associated with perturbation of the atom's electronic structure by an oscillating electric field and that field's change in strength as a function of location. For the nominal TEM_{00} laser spatial mode, the radial intensity derivative is negative. This leads to a positive force (in the radial direction) for positive detuning (blue) and a negative force for negative detuning (red). In other words, for red-detuned light, atoms would be drawn to the center of a Gaussian profile and vice-versa for blue-detuned light. To complete the dipole force derivation for simulation, the nominal TEM_{00} spatial mode given by

$$I(r) = C_1 e^{C_2 r^2} \Leftarrow C_1 = -\frac{P_L C_2}{\pi}, C_2 = -\frac{4\ln 2}{D_L^2} \tag{4}$$

where P_L is the laser power and D_L is the laser FWHM diameter. Equation (4) can then be inserted into (3) and subsequently integrated into the code.

METHODOLOGY

The primary tool for this investigation was a custom particle trajectory code which simulated the resonant interaction between a thermal [350 K] cesium atomic beam and a resonant laser field. In order to validate this code, an experiment was conducted which demonstrated the steering of an atomic beam using the photon scattering force, given above by equation (1). The experimental atomic beam was a geometrically skimmed thermal [373 K] cesium beam interacting with a laser field tuned near the D_2 cycling transition ($6s\ ^2S_{1/2}\ F = 4 \leftrightarrow F = 5\ 6p\ ^2P_{3/2}$) with a wavelength of 852.35 nm. A diagram of the experimental vacuum system can be seen in Figure 1 (A). The coldest point of the cesium oven, similar in design to [5], was actively controlled to 100°C by a tape heater and thermocouple. The shutoff/regulating valve and subsequent piping was kept at least 10°C warmer to avoid unwanted condensation. The effluence from the oven was differentially pumped and subsequently skimmed by a copper disk with a 1 mm orifice opposite the oven orifice. This setup created an atomic beam with a sufficiently small transverse velocity for the experiment. The separation between the oven and skimming orifices was approximately 260 mm. After passing through the skimming orifice, the atomic beam passed through the manipulating laser field (denoted by "Optical Interaction"). After this interaction, the beam was allowed to drift for approximately 450 mm before being irradiated by a second laser field (denoted by "Fluorescence Beam"), which induced fluorescence. This fluorescence was detected by a cooled CCD camera which recorded the beam's position.

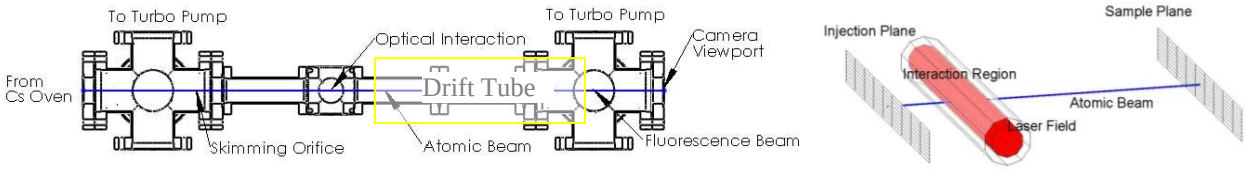

A B

FIGURE 1. A) Diagram of experimental vacuum system (side view) and B) Notional diagram of TCL code domain.

The laser system was comprised of a tapper amplified 852 nm diode laser in the Littrow/Metcalf configuration, manufactured by Sacher Lasertechnik GmbH. The line width of the laser was rated to approximately 1 MHz; however, the experiment suggests a broader line width. The laser light was passed through an acousto-optic modulator (AOM) in a double pass configuration [6]. The frequency shifted light was then passed to the experimental setup; it was split to act as both the optical interaction laser field (beam modification) and the fluorescent field (beam detection). The experimentally recorded Doppler-free saturation absorption spectroscopic profile from the laser's internal absorption setup can be seen in Figure 2 (A). The two end peaks and the shoulder correspond to transitions between the upper hyperfine ground state ($F = 4$) and the three allowed hyperfine excited states ($F = 3\ldots5$); the other three peaks are "crossover" peaks caused by the saturation absorption setup. The width of the cycling transition ($F = 4 \leftrightarrow F = 5$) for a perfectly monochromatic laser, in a truly Doppler-free non-power broadened spectroscopic setup, would be given by the natural radiative width of the transition, ~5.25 MHz. However, both the saturation absorption setup and the atomic beam fluorescence signal as a function of AOM detuning showed the width to be approximately four times wider than the natural width, as seen in Figure 2 (B).

A B

FIGURE 2. A) Saturated absorption signal and B) atomic beam fluorescence signals vs. frequency.

Numerical simulations were conducted using a custom Monte Carlo particle trajectory which simulated a pre-determined number of particle trajectories through a domain. At the end of the simulation, the final location of the recorded trajectories was gathered and used for sampling the horizontal spatial distribution of the particles at the sampling plane. The domain did not contain any formal geometry; a particle passed from injection to sampling, having only interacted with a laser field. The simulation represented the basic experimental setup described above. A notional diagram of the domain can be seen in Figure 1 (B). The injection surface of the code represented the skimmer surface, the origin of a directional flow. The particle's injection characteristics, position and velocity, were sampled from an analytical distribution representative of a free molecular, geometrically skimmed, vacuum effluence. The trajectory was assumed to be in free flight when not interacting with the laser field. While in the laser field, the force equations given above were used to solve a set of n-variable differential equations, via Gear's Method[*], which gave the particle's trajectory through the laser field.

RESULTS AND DISCUSSION

When considering the steering of an atomic beam with the photon scattering force, the intensity of the laser and the velocity of the atom, along the laser axis, directly affect the magnitude of the force. Referencing equation (1), the force exerted on a cesium atom at the center of a 25.4 mm Gaussian laser, locked to the D_2 cycling transition, as a function of the laser's power can be seen in Figure 3 (A). The force saturates at a value of 1.28×10^{-20} N, consistent with equation (2). After the limiting necessity of atom-laser systems with isolated (cycling) transitions, the inability to indefinitely increase the force on the atom is the greatest drawback to the use of the photon scatting force for steering atomic trajectories. For a laser tuned to the center of the transition, the velocity at which the atom is most likely to absorb a photon is 0 m/s. Doppler shifting of the incident photon, in the atom frame, decreases the likelihood of absorption, by increasing detuning, for all non-zero velocities, as seen in Figure 3 (B). When the laser

[*] HSL, A Collection of Fortran codes for large-scale scientific computation. See http://www.hsl.rl.ac.uk, (2007)

is detuned 20 MHz to the blue side (higher frequency) of the transition, the most likely velocity to absorb a photon is +17.05 m/s. This mechanism offers a straightforward velocity selection for photon scattering based laser momentum deposition (steering) or cooling (collimation).

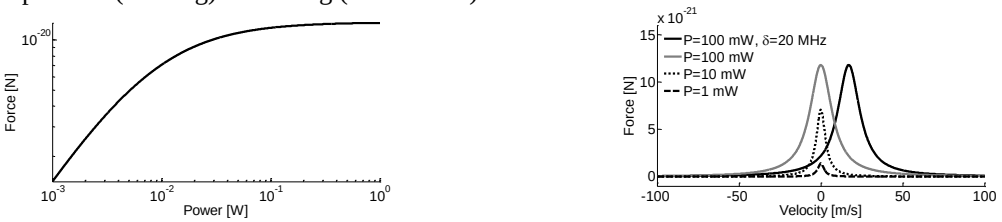

A B

FIGURE 3. Photon scattering force vs. A) incident laser power and B) vs. atom velocity

An example of the atomic beam spatial profile from the numerical simulations can be seen in Figure 4 (A) utilizing the photon scattering force. In this simulation the laser was assumed to be 13 mW, aligned left to right in the figure, perpendicular to the axial direction of the beam, and detuned to the blue side (higher frequency) of the D_2 transition by 1.1 MHz. The peak of the distribution shifted approximately 5 mm, or five times the full width half maximum of the original distribution. The magnitude of the spatial displacement was mainly a function of the amount of distance the atoms are allowed to drift after the interaction region. The change in the velocity distribution function is seen in Figure 4 (B). The center of the distribution shifted approximately 3.5 m/s, over 3 times the full width half max of the original distribution. This corresponds to a Doppler shift of approximately 4 MHz. The shift is consistent with the edge of the bandwidth where an atom accelerated itself out of resonance with the laser field, approximately half of the natural width (2.6 MHz) plus the laser detuning (1.1 MHz). It should be noted that the laser was simulated as a monochromatic source, i.e. a laser source with zero line width.

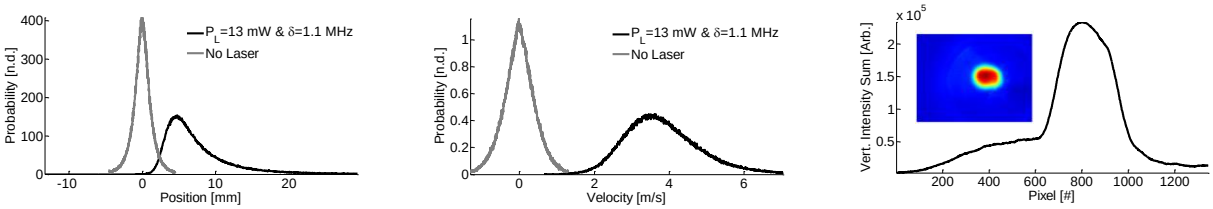

A B C

FIGURE 4. Atomic beam A) spatial B) velocity profiles after laser steering and C) Experimental vertical bin summing.

Figure 4 (C) inset shows the experimental atomic beam fluorescence signal from the cooled CCD. In order to compare the two-dimensional CCD intensity profile with the one dimensional numerical density profile, the experimental vertical intensity pixels were summed along the horizontal axis. An example of the vertical summing can be seen in Figure 3 (C). A Gaussian least-squares fit was consistently used for the numerical and experimental profiles in order to ensure consistent determination of the profile shifts. Figure 5 (A) shows the centers of least-squares fits from the numerical simulations, as a function of the incident laser detuning from the cycling transition frequency. A factor which limited the atomic beam deflection, for a constant frequency laser, was that the acceleration of the atoms along the laser propagation axis eventually moved the atoms out of resonance; thus the force on the atoms reduced as the atom accelerated. This led to an optimum frequency at which to set a constant-frequency laser. Slightly blue detuned light (higher frequency) balanced the desire to affect the largest number of initial atoms while allowing the atoms the largest bandwidth through which to accelerate before moving out of resonance.

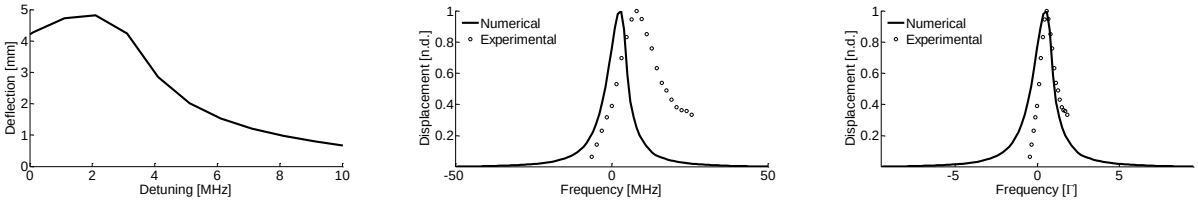

A B C

FIGURE 5. Numerically simulated atomic beam deflection vs. laser frequency and comparison with experiment.

In order to validate the trajectory code approach, the effect of incident laser frequency on the deflection of the atomic beam was experimentally demonstrated. The comparison between the numerical and the experimental

results can be seen in Figure 5 (B), normalized by the maximum displacement. The reason for the shift and broadening of the experimental points was the non-zero line width of the experimental laser. There was increased overlap between the frequencies of light emitted by the laser and the natural width of the transition, which broadened the bandwidth of laser frequencies accepted by the atom. When the frequency of the experimental points are normalized by the recorded Doppler-free saturation absorption width and the numerical profile is normalized by the assumed natural line width, seen in Figure 5 (C), the comparison shows much closer agreement. The agreement between the experiment and the numerically predicted peak validates the general use of the particle trajectory code, with integrated resonant interaction simulation capability, as a predictive tool.

Extending the use of the photon scattering force for the collimation of alkali atomic beams has been documented experimentally [7]. The process is known as a one-dimensional "optical molasses" because the laser fields act like a viscous fluid [1], retarding the velocity of the particles along the laser axis. In this configuration an additional laser was simulated to create two, counter propagating, non-interfering (in reference to their polarization vectors), laser fields, aligned perpendicular to an atomic flow. When both lasers were slightly red-detuned (lower frequency), atoms with velocities travelling against the propagation direction of each laser were preferentially selected for excitation. Subsequently, this added momentum counter to the atom's velocity, slowing it down. Figure 6 shows the width of numerically simulated atomic beams which have passed through such an optical molasses. The grey line represents the width of the atomic beam simulated without passing through the laser interaction. When the fields were detuned too far to the red (lower frequency), none of the atoms, at any velocity, were sufficiently in resonance to be strongly influenced by the lasers. As the frequency detuning was reduced (moving closer to the center of the graph), a larger fraction of the atoms were brought into resonance and the atomic beam became more collimated. After an optimal detuning, approximately $\Gamma/2$ or 2.62 MHz, the magnitude of the effect was reduced until it was reversed. When the lasers were blue detuned (higher frequency), the relevant velocity classes being Doppler shifted into resonance were reversed in sign. In this region, each laser began preferentially selecting atoms which were moving away from it, causing dispersion instead of collimation.

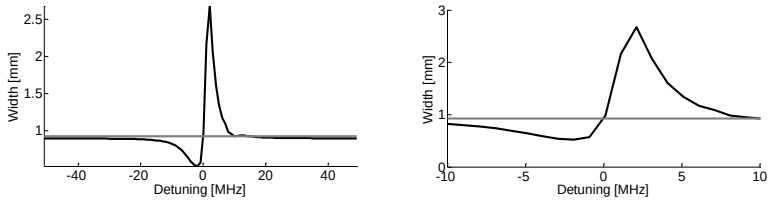

FIGURE 6. Atomic beam width vs. laser frequency for photon scattering collimation.

Unlike the photon scattering force, the use of the dipole force is not asymptotically limited as a function of the laser intensity and less stringently tied to Doppler shifting. While this process is applicable to all species subjected to an electric field, the magnitude of the effect is greatly enhanced when the irradiating laser field oscillates near an electronic resonance. Tuning the laser near resonance comes with a tradeoff; however, as the increased likelihood of photon absorption near resonance has a severe impact on the force. The derivation for the dipole force, given above, is for the force on an atom in the ground state; for an excited atom, the sign of the force is reversed. The relation of intensity to detuning in equation (3) suggests that there is an optimum combination of intensity (gradient) and detuning which provides for the maximum force with an acceptable likelihood of excitation. A ratio of the Rabi frequency to the detuning (Ω/δ) of 0.2, at the center of a 50 μm diameter, 100 W laser, represents a likelihood of excitation of approximately 1%. This requires a detuning of approximately 511 GHz. These laser parameters were used for simulations on the steering and collimation of an atomic beam, using the induced dipole gradient force.

The position of the laser relative to the center of the atomic beam was varied from -50 μm to 50 μm, in the vertical direction, orthogonal to the laser axis and the atomic beam axis. The deflection of the atomic trajectories versus laser position can be seen in Figure 7 (A). The shape adequately traces the intensity gradient of the laser field intensity in the vertical direction. It can also be seen that, while the laser was near the centerline, there was a fairly linear relation between the position of the laser and the deflection of the atomic beam. This is advantageous for micro-machining applications which require fine control of the atomic flow for micron and sub-micron feature sizes. Additionally, the simulations showed a change in the width of the atomic beam as a function of laser position. Figure 7 (B) shows the width of the spatial profile, versus the position of the laser field. The grey line represents the un-perturbed width of the atomic beam. The laser positions which resulted in the most dispersion of the beam were the positions which imparted the most deflection on the beam. At these positions, the force on an individual portion of the atomic flow was different according to that portion's entry into the field. When atomic beam entered the laser such that the greatest deflection was obtained, there was also the greatest difference between the forces acting on the top of the atomic beam and the forces on the bottom of the beam. When the position of the center of the laser field

was aligned with the axis of the beam, the divergence of the atomic beam was cancelled by the bending of the atomic trajectories through the laser field, like focusing rays of light through a lens.

A B

FIGURE 7. Atomic beam A) center and B) width vs. laser vertical position for resonant dipole steering and collimation.

CONCLUSION

A numerical study was conducted on resonant laser atomic beam manipulations, utilizing the photon scattering and resonant induced dipole force. The representative test cases investigated in this study, related directly to flows associated with micro-machining, micro-engineering, and continuing application in the area of atomic physics and spectroscopy. Simulations were conducted using a custom particle trajectory code, which simulated a rarefied cesium atomic beam interacting with a Gaussian resonant laser field. A validating experiment, which used a narrow line width, external cavity, tunable diode laser to impart momentum to the cesium beam, was also conducted. The numerical simulations showed good agreement with the validating experiment when experimental factors, such as the finite line width of the laser, were taken into account. Limitations associated with steering and collimation of the atomic beam using the photon scattering force were shown to be associated with the asymptotic relation of the force and laser intensity and with directional acceleration due to a fixed frequency laser. Despite these limitations, the photon scattering force was numerically simulated and experimentally demonstrated to be capable of steering a cesium atomic beam as a function of the laser frequency with a maximum beam displacement being identified for slightly blue detuned laser light. When used for beam collimation, the photon scattering force was shown to reduce transverse velocity for red detuned light while increasing dispersion for blue detuned light. Limitations associated with steering and collimation of the beam using the induced dipole force were shown to be associated with the small scales required to create a strong laser field intensity gradient and with the tuning of the laser field properties to properly focus the atomic beam through the laser fields.

ACKNOWLEDGEMENTS

This work has been supported by the Air Force Research Laboratory at Edwards AFB, CA and the Air Force Office of Scientific Research. The authors wish to thank Dr. Ingrid Wysong for her continued support and input. The authors also wish to thank the ERDC DoD Supercomputing Resource Center (DSRC), particularly David Dumas, for their cooperation and aide in conducting part of the numerical simulations.

REFERENCES

1. Chu, S., et al., *Physical Review Letters* **55**, 48 (1985).
2. Gordon J. P. and Ashkin A., *Physical Review A* **21**, 5 (May 1980), pp 1606-1617.
3. Steuernagel, O. *Journal of Optics A* **7**, 6 (May 2005), pp S392-S398.
4. Metcalf and van der Straten, Laser Cooling and Trapping, New York, NY: Springer-Verlag New York, Inc., 1999.
5. Tompa G. S., Lopes J. L., and Wohlram G., *Rev. of Sci. Instr.* **58**, 8 (August 1987), pp 1536-1537
6. Donley E. A., et al. , *Rev. of Sci. Instr.* **76**, 6 (June 2005), pp 063112
7. Rehse S. J., Bockel K. M., Lee S. A.. *Physical Review A* **69**, 06 (June 2004), pp 063404